Experimental Mechanics (2010) 50:1183–1197
DOI 10.1007/s11340-009-9316-8

An Experimental and Numerical Study of *Calliphora* Wing Structure

R. Ganguli · S. Gorb · F.-O. Lehmann · S. Mukherjee · S. Mukherjee

Received: 9 March 2009 / Accepted: 9 November 2009 / Published online: 20 November 2009
© Society for Experimental Mechanics 2009

Abstract Experiments are performed to determine the mass and stiffness variations along the wing of the blowfly *Calliphora*. The results are obtained for a pairs of wings of 10 male flies and fresh wings are used. The wing is divided into nine locations along the span and seven locations along the chord based on venation patterns. The length and mass of the sections is measured and the mass per unit length is calculated. The bending stiffness measurements are taken at three locations, basal (near root), medial and distal (near tip) of the fly wing. Torsional stiffness measurements are also made and the elastic axis of the wing is approximately located. The experimental data is then used for structural modeling of the wing as a stepped cantilever beam with nine spanwise sections of varying mass per unit lengths, flexural rigidity (EI) and torsional rigidity (GJ) values. Inertial values of nine sections are found to approximately vary according to an exponentially decreasing law over the nine sections from root to tip and it is used to calculate an approximate value of Young's modulus of the wing biomaterial. Shear modulus is obtained assuming the wing biomaterial to be isotropic. Natural frequencies, both in bending and torsion, are obtained by solving the homogeneous part of the respective governing differential equations using the finite element method. The results provide a complete analysis of *Calliphora* wing structure and also provide guidelines for the biomimetic structural design of insect-scale flapping wings.

Keywords Micro air vehicle · *Calliphora* · Mass per unit length · Flexural rigidity · Torsional rigidity · Natural frequency · Finite element method

R. Ganguli (✉) · S. Mukherjee
Department of Aerospace Engineering,
Indian Institute of Science, Bangalore, India
e-mail: ganguli@aero.iisc.ernet.in

S. Gorb
Evolutionary Biomaterials,
Max Planck Institute for Metal Research,
Stuttgart, Germany

F.-O. Lehmann
Biofuture Research Group, Institute of Neurobiology,
University of Ulm, Ulm, Germany

S. Mukherjee
Department of Civil Engineering,
National Institute of Technology,
Tiruchirappalli, India

Nomenclature

A	area
b	width
E	material stiffness (Young's modulus)
EI	flexural rigidity
f	force per unit length
f_0	torque per unit length
F	applied force
G	shear modulus
GJ	torsional rigidity
h	thickness
i	imaginary unit
I	moment of inertia
I_0	mass polar moment of inertia per unit length
J	polar moment of inertia
k	bending stiffness

K	global stiffness matrix
l	mean section length
m	mass per unit length
$\bar{m}$	average mass of each segments
M	global mass matrix
Q	nodal displacement vectors
t	time
x	distance
y	deflection in y-direction
y_{tip}	deflection at the tip
ρ	density
σ	Poisson's ratio
ω	natural frequency

Introduction

There is a world wide interest in the development and further research on a family of very small size air vehicles having a maximum dimension of 15 cm and a gross weight of 100 g known as Micro Air Vehicles (MAVs). The three main approaches for providing lift for such vehicles are through fixed, rotating and flapping wings. Fixed wings lack low speed flight capability which may be critical for MAVs in indoor situations. Rotary wing can lead to significant noise signatures. Nature provides numerous flying birds and insects which use the flapping wing technology [1, 2]. In fact, one can consider birds and insects to be naturally designed flapping wing micro air vehicles. Therefore, it is of great interest to study natural flyers for insights into biomimetic MAVs [3, 4].

The main mission of MAVs is flying in confined spaces inside buildings, shafts, tunnels, machine rooms etc. This requires power-efficient, highly maneuverable and low speed flight. Such performance is routinely exhibited by flying insects. In particular, flying insects have fascinated MAV researchers because of their excellent flying characteristics. A detailed discussion of the future utility of MAVs and the advantages of considering insect-like flapping wing propulsion has been presented by some researchers [5–7]. Research has also been done on the propulsion and aerodynamics of flapping wings [8–11]. The objective of much of this work is to understand the fundamental physics behind insect flight which typically occurs at Reynolds number of $10 - 10^4$. Another objective is to develop analytical and numerical models which can be used for the design of insect like MAVs. An important feature of flapping flight aerodynamics is their unsteadiness and formation of a leading edge vortex on the wing. These effects are in addition to the conventional wake shed from the trailing edge of the wing. The modeling effort is therefore complicated. A recent and comprehensive review of insect flight aerodynamics is provided by Wang [12].

Relative to the large number of works on insect flight aerodynamics, very few researchers have focused on insect wing structure. In fact, biological structures are complex composite structures and show very good mechanical properties even though they are made from weak materials [13]. In general, insect wing structures are composed of membranes strengthened by veins. Wang et al. [14] found that the dragonfly veins are complex microstructures consisting of chitin shell, muscle and fibrils. The vein structures are such that they allow the insect to sustain high levels of bending and torsion loads. In another work, Machida et al. [15] found that the costal vein plays an important role in the bending and torsion of the dragonfly wing.

Since the insect wing is a complex mechanical structure, some researchers have modeled it using the finite element method. For example, Smith [16] modeled the veins as three dimensional tubular beam elements of varying thickness for the hawkmoth *Manduca Sexta*. Wootton et al. [17] modeled the wing membrane using orthotropic plane stress quadrilateral (or triangular) elements of varying thickness. Wooton et al. [17] also summarize the current work on the structural modeling of insect wings and show how research has progressed from simple conceptual models of the wing structure to analytical methods and numerical approaches based on the finite element method. A limitation of some of these works is that detailed information about the material and geometric properties of the veins and membranes along the complete wing are required for developing a finite element model.

Another approach for modeling the wing mechanics is to obtain equivalent beam-type variation of the overall stiffness properties experimentally. Taking this approach of experimental work, Combes and Daniel [18, 19] estimated the distribution of flexural stiffness in the dragonfly *Aeshna Multicolor* and the hawkmoth *Manduca Sexta* and approximated the variation as an exponential decline from the wing root to tip. They attached the fresh wings at the root using wax and applied loads at selected sections of the wings to obtain the stiffness properties. They found that the different insects studied followed the general pattern of high stiffness near the wing root and low stiffness near the tip. In addition, they performed finite element simulations using the experimental data and showed considerable levels of wing deflection resulting from distributed lifting forces acting on the wing and needed to support the insect weight. However, Combes and Daniel [18, 19] did not investigate the mass variation along the wing. The variation of mass per unit length along

Fig. 1 Magnified view of blowfly *Calliphora*

with wing is needed for structural dynamic analysis. As we will see later in this paper, the governing partial differential equations for bending and torsion of beams require mass per unit length and torsional inertia distribution, respectively. While they measured the out-of-plane and in-plane stiffness, they did not measure the torsional stiffness. Ennos [20–22] studied the effects of the torsional rigidity of the insect wings on aerodynamic efficiency. Sunada et al. [23] looked at the torsional deformation and stiffness of dragonfly wings. They found that wing corrugations cause an increase in torsional stiffness due to warping effects. It is clear from videos of flying insects that elasticity plays an important role in insect wings. For example, during stroke reversals, torsional stiffness is important. Recently, Rosenfeld and Wereley [24] studied structural parametric stability of flapping insect wing. They developed a linear time-periodic assumed-mode analysis by modeling the wing structure as a thin beam. The effects of normalized cantilever frequency, bending modes, torsion modes, feathering stroke, location of cross sectional center of gravity and the location of feathering axis on the time periodic stability are shown. In general, a study of the structural aspects of biosystems is becoming increasingly important [25, 26].

In this paper, we present experimental results for mass and stiffness distributions of the wings of the blow fly, *Calliphora*, a picture of which is shown in Fig. 1 (figure from *wikepedia.org*) and subsequently model the wing into a non-uniform cantilever beam. Since flies are very agile fliers, they are a source of inspiration for micromechanical insect design [27, 28]. While most MAV researchers simply want to construct a flapping wing MAV and do not seek significant levels of biomimesis, a close duplication of insect wings may yield advantages over a new design. It can be seen from Fig. 1 that the fly represents a complete miniature aerospace system, with wings for providing lift and controllability, a vision and nervous system for navigation and guidance, and a body as the payload. Therefore, it allows one to take advantage of the evolutionary design by nature which occurred over very large time scales.

Experimental Data

A microscopic view of the fly wing is shown in Fig. 2. For later use in obtaining stiffnesses along the wing span, we define three radial locations as basal, medial and distal based on wing venation patterns as shown in Fig. 2.

The wing was divided into nine spanwise (1 at tip and 9 at root) and seven chordwise regions (1 at trailing

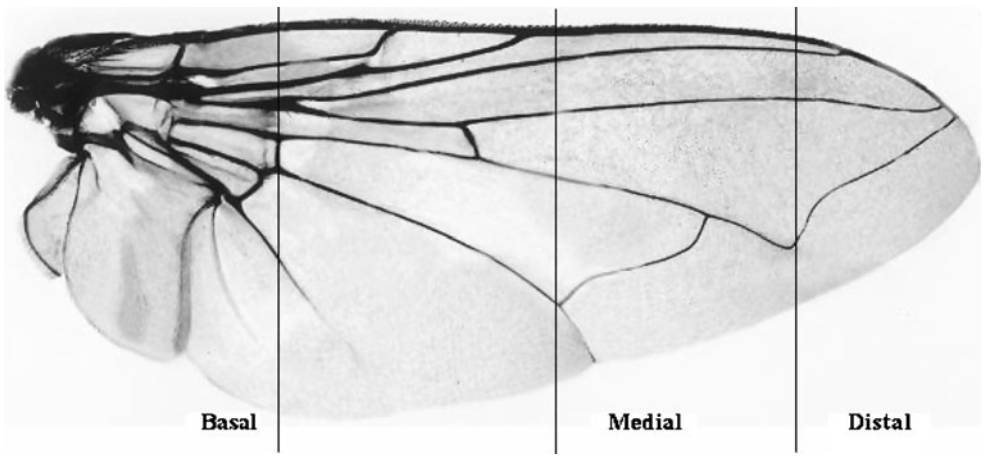

Fig. 2 Magnified view of *Calliphora* wing with the three stiffness measurement locations

edge and 7 at leading edge) based on venation patterns, as shown in Fig. 3. Since biological systems have considerable scatter, we used fresh wing for each measurement. Both wings of 10 male flies were measured, resulting in a total of 20 wings. The average weight of the flies is 59.0867 mg with a 95% confidence interval based on the t-distribution being [51.7901 mg, 66.3833 mg]. The weights of the 10 specimen varied from a low of 44.0523 mg to a high of 76.2182 mg with a standard deviation of 10.2097 mg.

Wing Mass Distribution

The mass measurements are performed using a UMX2 weighing scale manufactured by Mettler Toledo and capable of measuring up to 0.1 μg. The insect wings were cut using special razor blades, manufactured by Ted Pella Inc., under a microscope with a magnification of 3000 and each wing segment weight was measured.

The data for the mass variation for the right wing is shown in Fig. 4 and for the left wing in Fig. 5. There is a clear increase in mass at the root compared to the tip. This variation is similar to that seen in airplane wings and helicopter rotor blades. The differences between the measurements are likely due to measurement error due to loss of fluids from the veins when the wings are cut and some variation in the precise location of the cut which has to be made carefully using razors. Also, there is natural variation present in biological systems. However, the overall trends and values of the mass at different locations show a clear pattern.

Results from the 10 pairs of wings are used to obtain average values and standard deviations. The average weight of the wing is 238.7 μg, or about 0.4% of the insect weight. The 95% confidence interval using the t-distribution is [228.07 μg, 249.33 μg]. Thus the wings perform a very important function of providing lift with a very low weight. However, biological systems show considerable scatter as individual flies have different weights and are at different stages of their development. The wing weights vary from a minimum of 200.3 μg to a maximum of 272.3 μg with a standard deviation of 22.94 μg. Figure 6 shows the mean and the confidence interval for 95% using t-distribution. Again, the higher wing mass near the root can be observed.

The chordwise mass distribution was obtained by cutting wings into seven locations. The seven sections are shown in Figs. 7 and 8 for the right wing and the left wing, respectively. In this case, section 6 near the leading edge of the wing has the highest mass. The high masses are also related to the presence of veins in the section as the veins contribute more weights than the

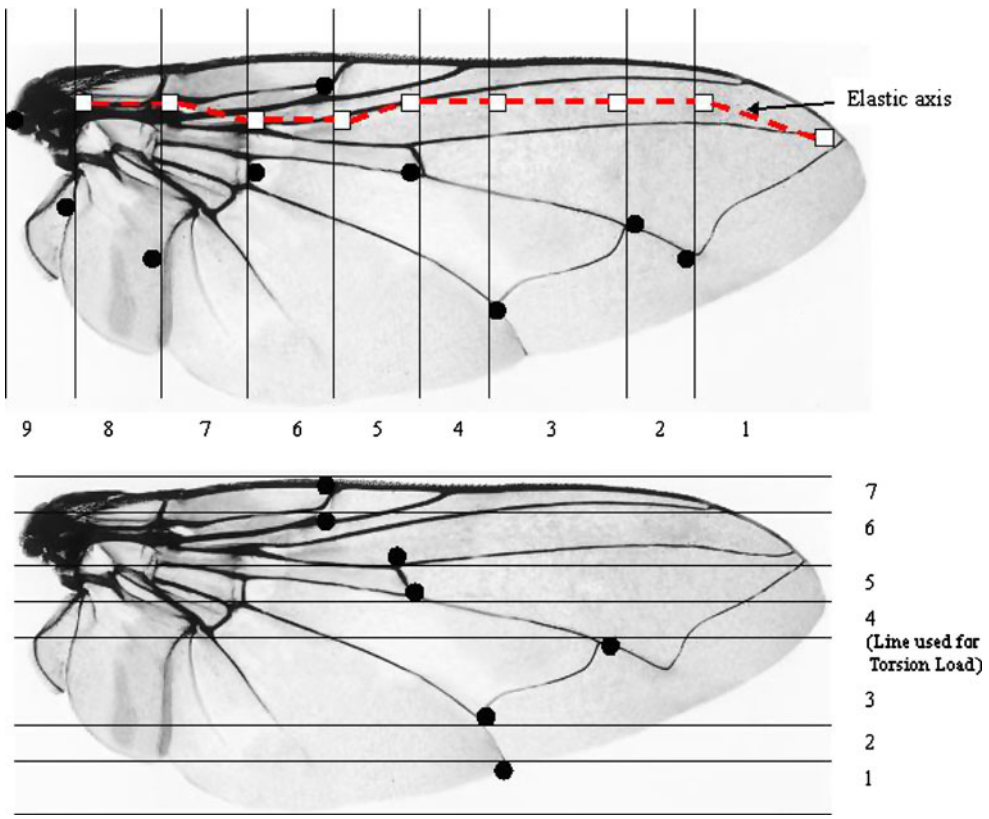

Fig. 3 Spanwise and chordwise locations used to cut wings for mass measurements. Intersection of the veins used as landmark points (*black circles*) which serve as guidelines to divide the spanwise and chordwise regions

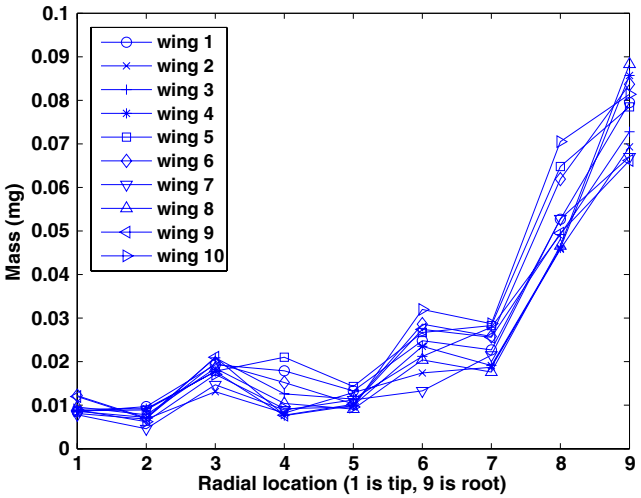

Fig. 4 Spanwise variation of mass along right wing for ten flies

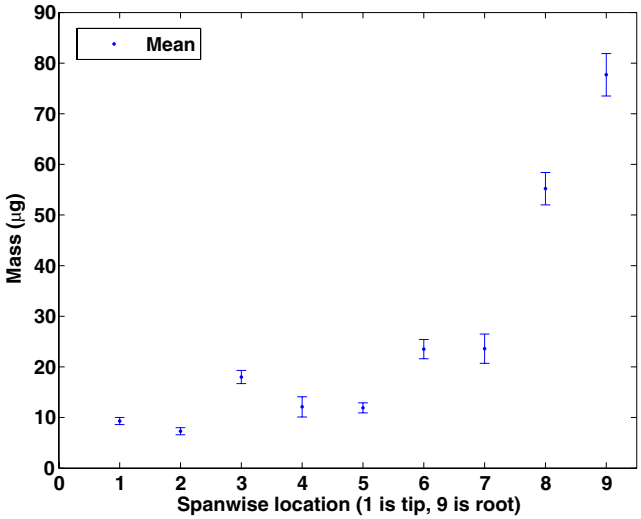

Fig. 6 Mean with 95% confidence interval based on the t-distribution for mass along wing span

membrane structure, which is very light. This can be seen from the low weights of sections 1 and 2 near the trailing edge of the wing which are composed of membrane material.

The mean for the chordwise mass with their 95% confidence intervals based on t-distribution is shown in Fig. 9. The trend seen from the raw data is now clearly noticeable. Since biological systems have considerable scatter, the mean values can be taken as wing design guidelines by engineers.

While every effort was made to cut the wings into sections in a clean manner, some loss of fluids from the veins as well as due to evaporation is inevitable. To quantify the loss, the whole wing weight prior to cutting it was measured and compared to the sum of the sectional cut weights. Figure 10 shows the mean value of the whole wing weights with the sum of the weights of the cut sections along with their confidence interval for 95% using the t-distribution. An average mass loss of about 18% results due to the cutting procedure. This kind of mass loss due to desiccation has also been observed by Ennos [21], who used the mass loss of about 10% to adjust the measured weights. We can also adjust the mean weights used for modeling by multiplying all the section weights by a factor of 1.18.

Geometry

The sectional weights do not indicate the true mass per unit length of each section as the different sections have

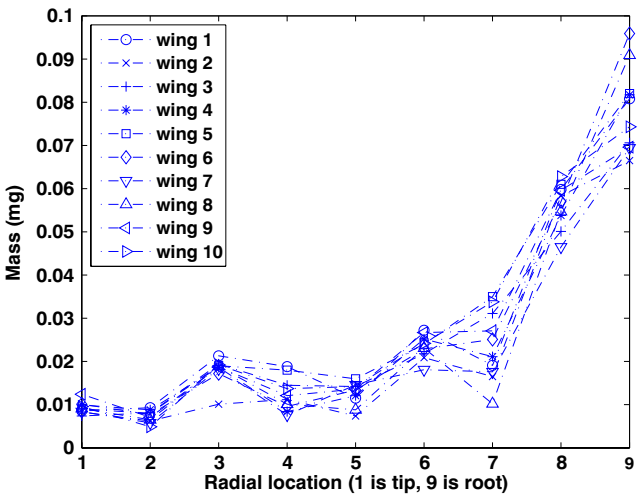

Fig. 5 Spanwise variation of mass along left wing for ten flies

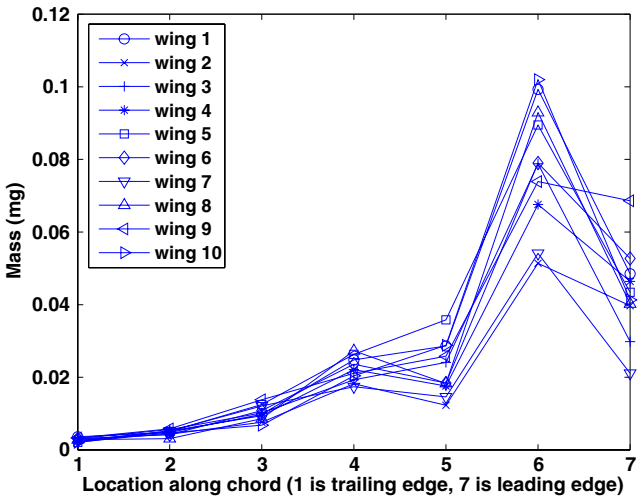

Fig. 7 Chordwise variation of mass on right wing

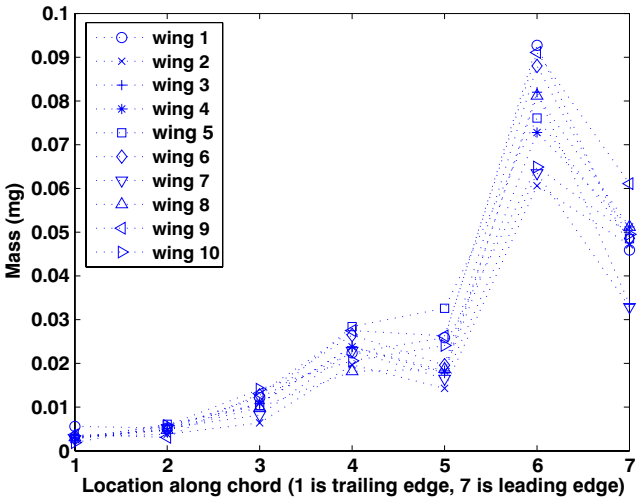

Fig. 8 Chordwise variation of mass on left wing

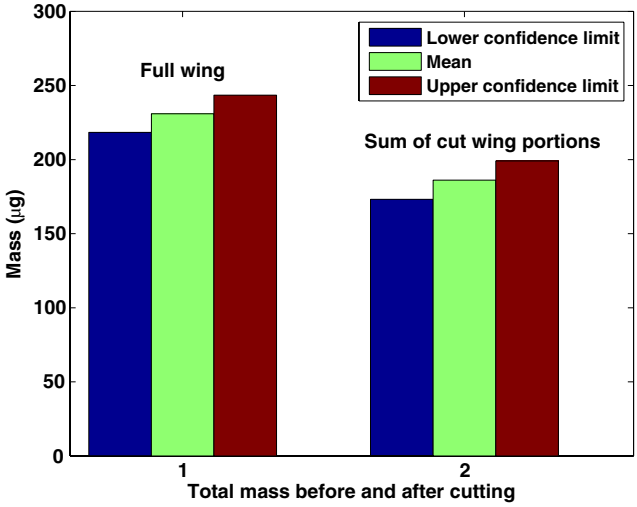

Fig. 10 Average mass loss in wing weight after cutting

different lengths, as can be seen in Fig. 3. To obtain the mass per unit length, which is the quantity used for engineering beam design, we measured the section lengths of 10 fly wing pairs.

A Mitutoyo precision microscope was used to measure the lengths of the nine spanwise and seven chordwise stations used for obtaining the mass distributions. These measurements provide a way to extract the average mass per unit length from the mass measurements. Also, they provide the distances between different vein junctions and therefore define the wing geometry. Figures 11 and 12 show the lengths with their 95% confidence intervals using Student's t-distribution along the spanwise and chordwise directions, respectively.

The wings ranged in length from a minimum of 7.46 mm to a maximum of 9.30 mm and the average length is 8.42 mm. The width ranges from a minimum of 3.07 mm to a maximum of 4.038 mm with an average width of 3.61 mm.

Mass Per Unit Length

The mass per unit length (m_i) at each section is calculated by dividing the average values of the mass ($\bar{m}_i$) with the average value of the length (l_i) of the section, which can be written as

$$m_i = \frac{\bar{m}_i}{l_i} \tag{1}$$

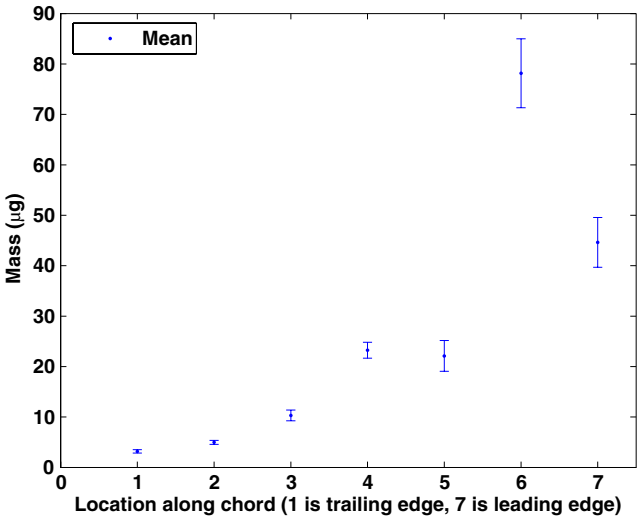

Fig. 9 Mean with 95% confidence interval based on t-distribution for mass along wing chord

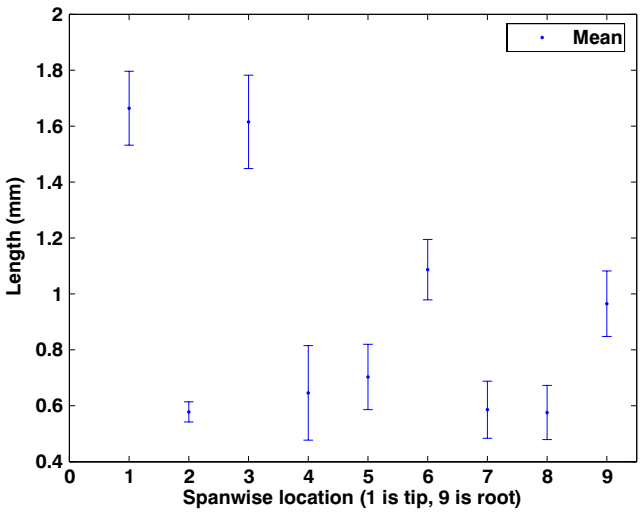

Fig. 11 Mean with 95% confidence interval based on t-distribution for length of wing spanwise sections

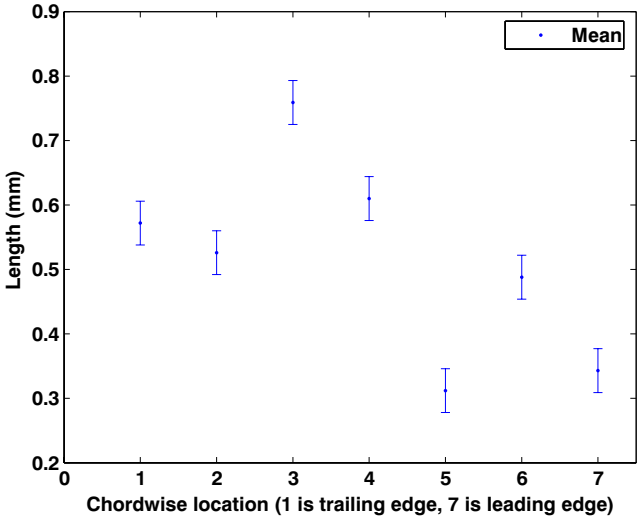

Fig. 12 Mean with 95% confidence interval based on t-distribution for length of wing chordwise sections

The mass per unit length distribution along the span is shown in Fig. 13. The highest mass occurs near the root region where the wing has to be structurally equipped to sustain higher stresses. The outer sections are much lighter in weight.

Figure 14 shows the calculated mass per unit length along the chord direction. The wing sections near the trailing edge have very low weight as the region is composed mostly of membrane material. The weight increases near the leading edge and is highest at section 6 which contains considerable vein material.

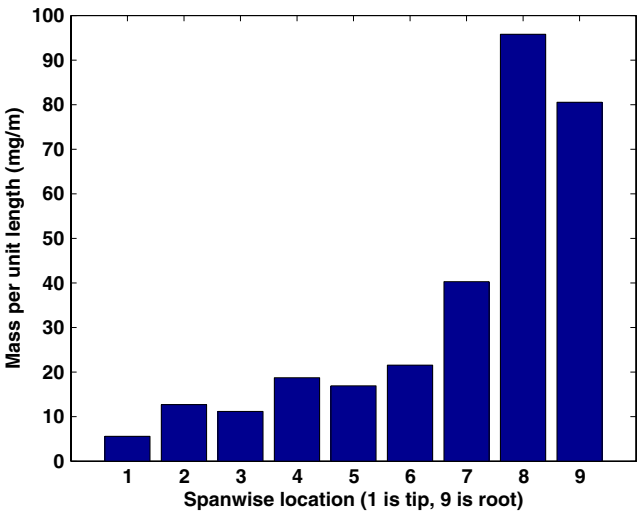

Fig. 13 Mass per unit length along wing span

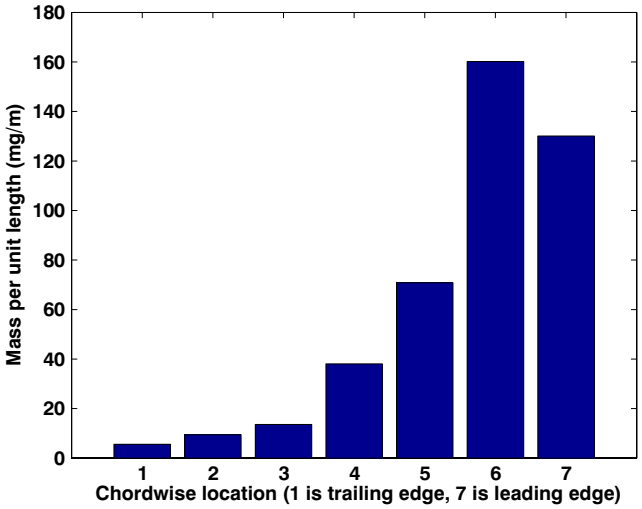

Fig. 14 Mass per unit length along wing chord

Bending Stiffness Distribution

For stiffness measurements, the wing is attached at the root to a holding device. Wax is used to attach the wing. The experimental setup which is used to perform

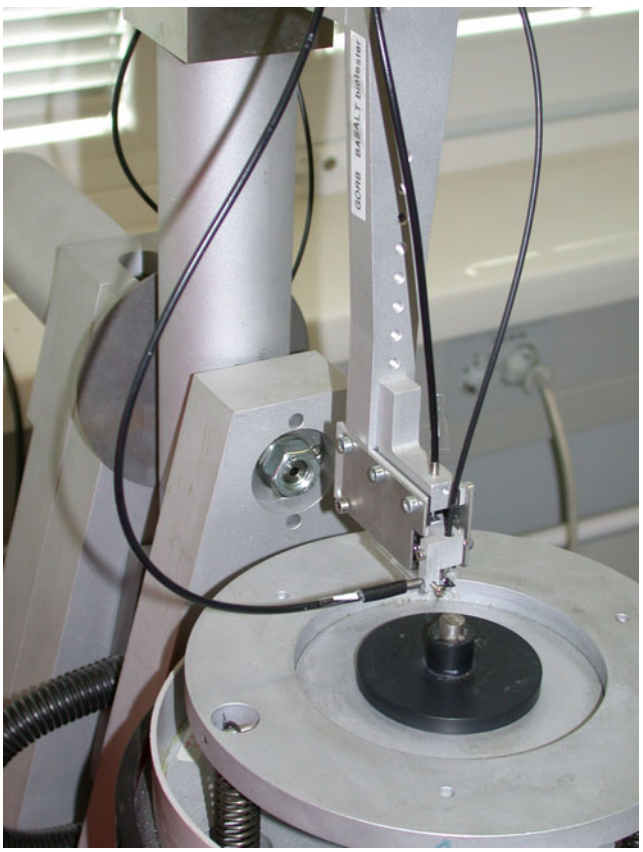

Fig. 15 Experimental setup used for stiffness measurements

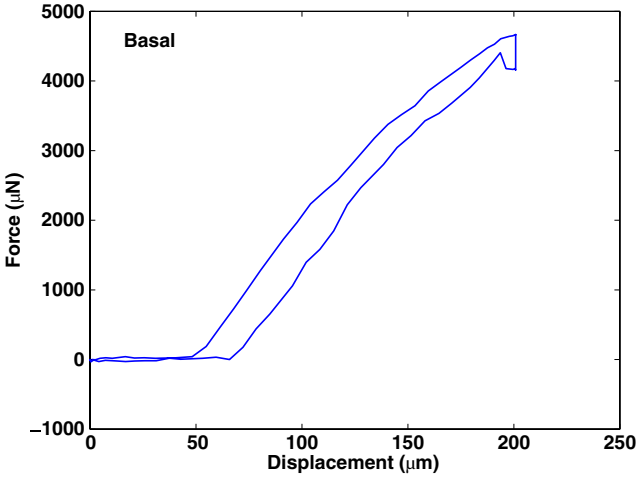

Fig. 16 Load versus displacement curve for basal location

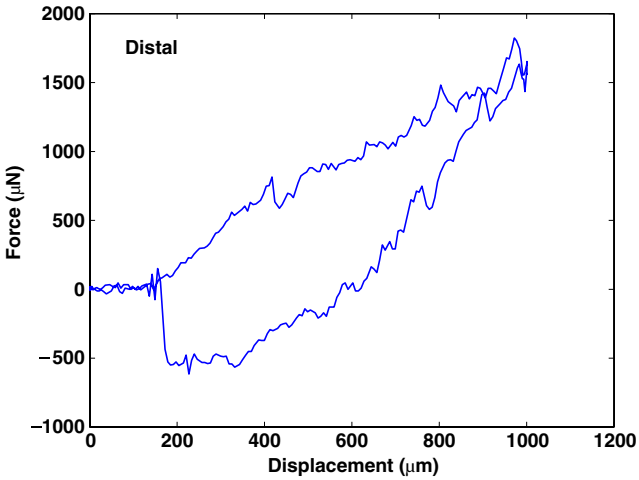

Fig. 18 Load versus displacement curve for distal location

the stiffness measurements is shown in Fig. 15. Force measurements were carried out with load cell force transducer (Biopac System Ltd., California, USA) using software AcqKnolwedge 3.7.0. The variable range force transducer incorporates a unique design which allows the transducer to cover a wide range of forces. AcqKnowledge is an interactive and intuitive program which is used to view, measure, analyze and transform data. Complex data acquisition and analysis can be performed using simple pull down menus and dialogs without using any programming language. Further details about the stiffness measurements are given in papers by Gorb and his co-workers [29, 30] who have used these extensively for biological measurements. In order to measure the bending stiffness, a load is applied to the wing at three locations shown in Fig. 2 (basal, near the root; medial, near the middle; and distal, near the tip). The load is applied using a rectangular blade with a length greater than the wing width such that pure bending motion is obtained. The load versus displacement curve for basal, medial and distal locations are shown in Figs. 16, 17 and 18, respectively. The linear region during the loading phase is used to determine the stiffness. The stiffness is measured for both downward and upward bending as preliminary load applications showed that the stiffness is different in these directions. Figure 19 shows the average values for the bending stiffness measurements with 95% confidence intervals using t-distribution when the load was applied from up so as to bend the wing down. Figure 20 gives the corresponding results for the bending up case. The stiffness is higher in the basal or root region of the wing and

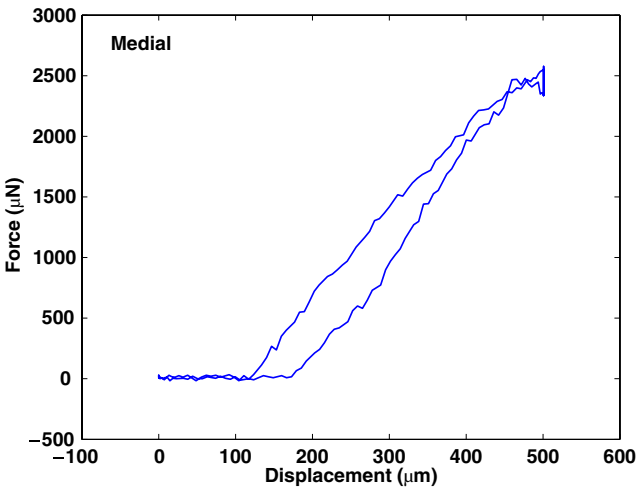

Fig. 17 Load versus displacement curve for medial location

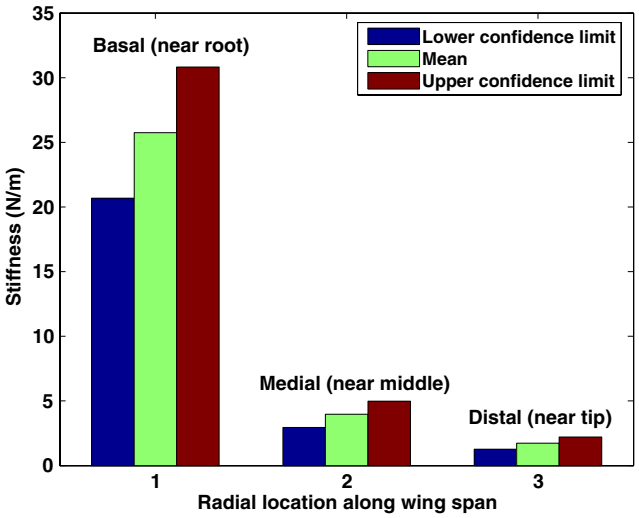

Fig. 19 Bending stiffness variation along wing when loading causes downward bending deflection

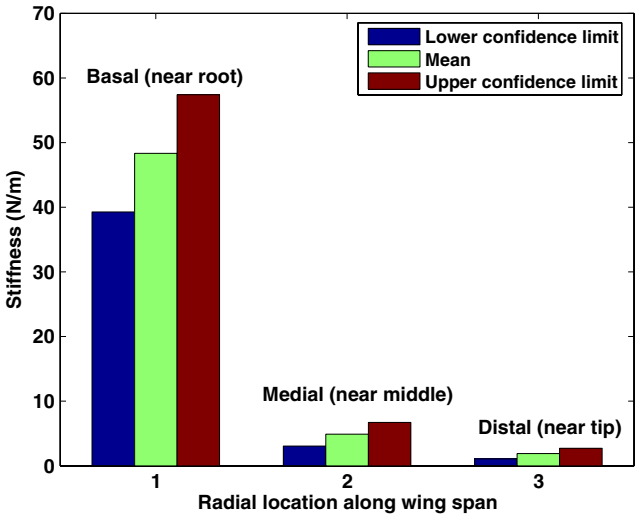

Fig. 20 Bending stiffness variation along wing when loading causes upward bending deflection

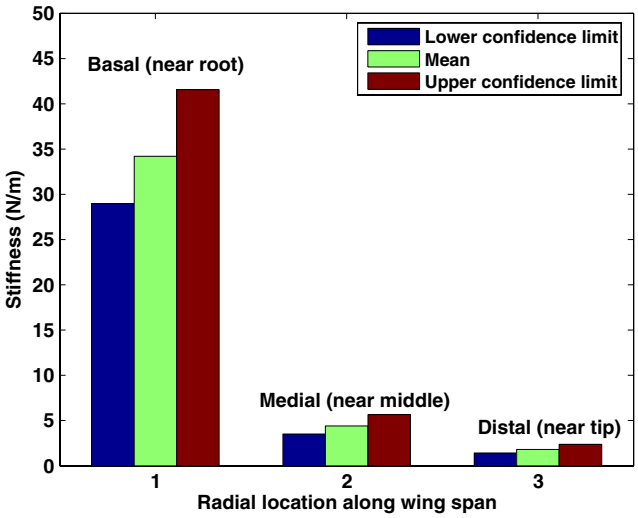

Fig. 21 Mean bending stiffness variation along the wing

falls dramatically towards the tip region. Though both sets of data show substantial scatter, it can be seen that the wing is stiffer when bending up compared to when bending down, especially near the basal region. The 10 pairs of wings tested in this case had minimum and maximum values of stiffness as shown in Table 1. The mean bending stiffness with 95% confidence intervals based on t-distribution for three radial locations on the wing is given in Fig. 21.

Torsional Stiffness

The torsional stiffness measurements are performed as follows. First, the elastic axis of the wing is determined in an approximate manner following the procedure outlined by Sunada et al. [23]. A needle is used to apply a load at different spanwise locations. At each spanwise location, the point where only bending resulted with the applied load is found. These points are then connected to determine the elastic axis. The elastic axis is found to be close to the leading edge of the wing, as shown in Fig. 3.

Following the determination of the elastic axis, a measure of torsional stiffness is obtained by applying a load along a line on the wing span at about two-third chord distance from the leading edge. This line is shown in Fig. 3. Again, as in bending, measurements are made for both upward and downward twist. The data obtained for the applied force divided by distance traversed at that point is then converted to torsional stiffness by using the distance between the elastic axis and the point of force application. Figure 22 shows the average values for the torsional stiffness with 95% confidence intervals based on Student's t-distribution. While there is considerable scatter in the data, the wing appears to be stiffer when twisting nose up compared to when twisting nose down. The anisotropy of the wing in bending and torsion may be related to the camber

Table 1 Minimum and maximum bending stiffness for 10 pairs of wings

	Basal (min, max)	Medial (min, max)	Distal (min, max)
Bending up (N/m)	19.097, 64.305	0.826, 12.37	0.457, 2.736
Bending down (N/m)	12.236, 48.011	1.01, 7.695	0.529, 4.478

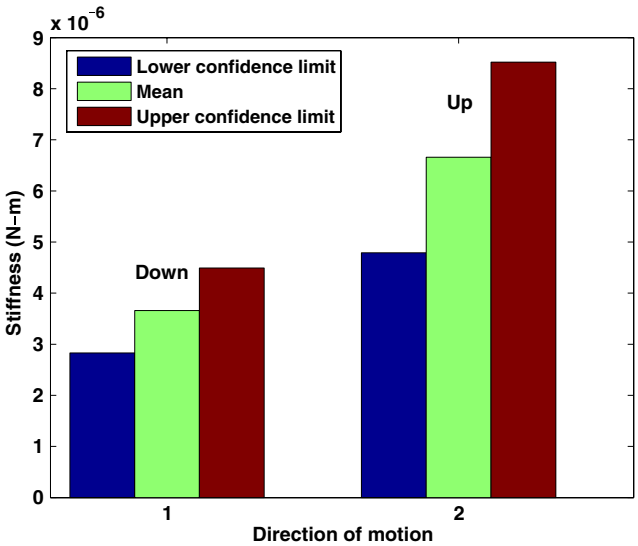

Fig. 22 Average torsional stiffness of wing

inherent in the insect wing. Its emulation for insect flight MAV is complicated but may be useful.

Structural Modeling of *Calliphora* Wing

The insect wing was modeled as a non-uniform cantilever beam and schematic diagram is shown in Fig. 23. It is required to estimate the geometric parameters, such as length, width and thickness along the span, for the numerical study of the non-uniform cantilever wing. However, length of each section of the non-uniform cantilever wing has already been obtained and is shown in Fig. 11. In order to estimate other two geometric parameters, the mass per unit length data from Fig. 13 is multiplied by the correction factor 1.18 as mentioned earlier to give the equivalent mass per unit length of the spanwise beam sections. This is represented in Fig. 24 and it accounts for the loss in mass due to cutting of the wings.

The equivalent beam segment areas (A_i) are obtained by taking the ratio of mass per unit length of the beam sections, as shown in Fig. 13 in discrete form, with the density of the material (ρ) as expressed by the equation

$$A_i = \frac{m_i}{\rho} \tag{2}$$

The element density is taken to be 1200 kg/m^3, as is typical of insect wings [18]. The data showing variation of areas is plotted in Fig. 25. The mean area was found to be about 0.03315 mm^2 with a standard deviation of 0.0032 mm^2. The 95% confidence interval using the Student's t-distribution is [0.0105 mm^2, 0.0557 mm^2].

For calculation of the beam widths, we formed a mesh on the wing consisting of nine spanwise and seven chordwise sections. We intended to get the best fit rectangles out of the spanwise beam sections. To do this, we took the chordwise width at the center of each spanwise section. We physically measured the span widths in a photograph of the wing that had maintained its original aspect ratio, and obtained a scale factor for cut portions towards the leading and the trailing edge. We multiplied the scale factor for the cut portions with their mean section widths and summed the inner chordwise section widths to get the beam segment width. For example, in Fig. 26, to calculate beam width of section 1, we drew a center line dividing span 1. The beam width would be width of span 4 and span 5 along with the abridged portions of span 3 and span 6. In the wing photograph, for chordwise section 3, we measured the length of the wing portion within the section along the center line and the total length of the chordwise section. Their ratio gave us the scale factor which we multiplied by the mean width of section 3 obtained from experiments. Similar procedure was done for section 6 towards the leading edge. This method was adopted for all the spanwise sections to get the beam widths. The calculated width data is given in Fig. 27.

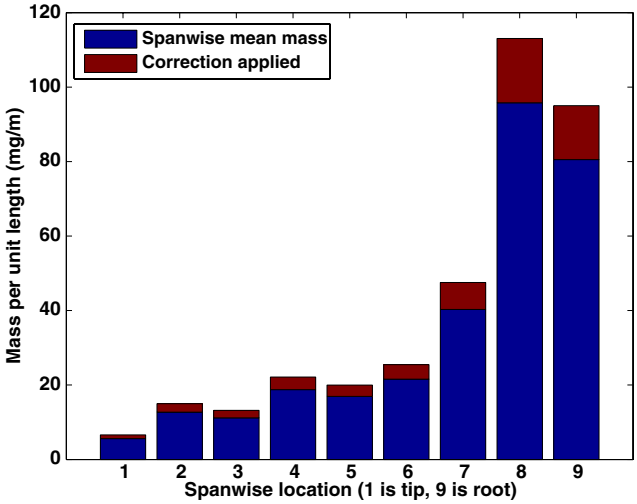

Fig. 24 Mass per unit length of spanwise beam segments

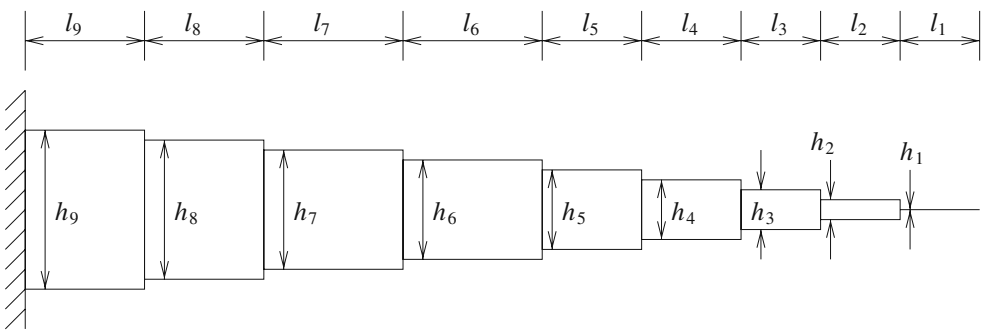

Fig. 23 Schematic diagram of non-uniform cantilever beam used for structural modeling of *Calliphora* wing

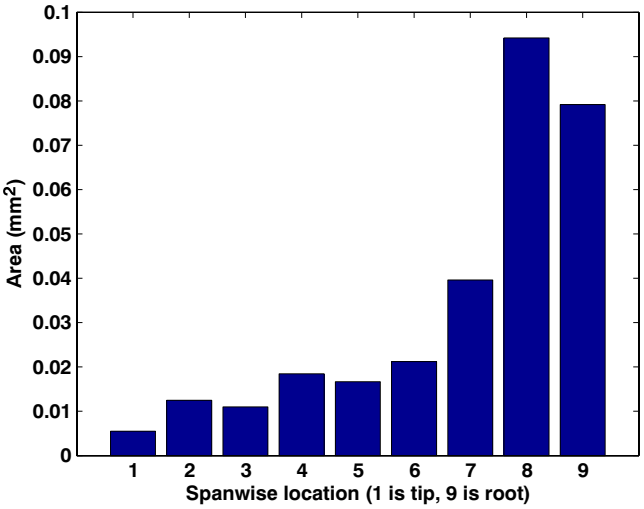

Fig. 25 Variation of area in spanwise beam segments

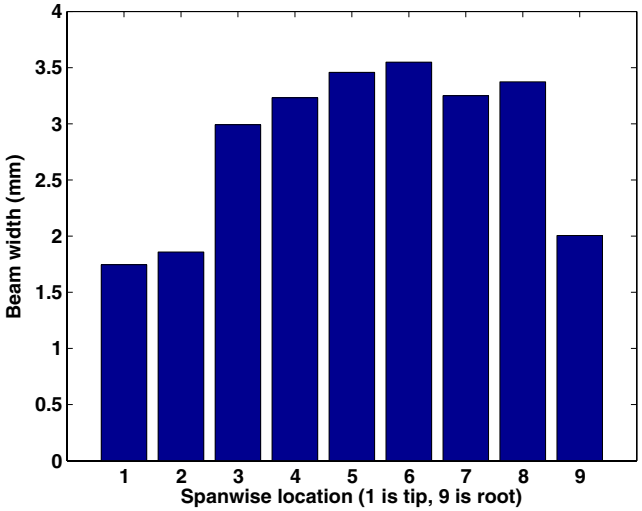

Fig. 27 Spanwise beam widths

A mesh is formed with seven chordwise and nine spanwise sections. In our quoted example, in calculation of beam width of span section 1, we use the expression

$$b_1 = \frac{a}{b} \times l_6 + l_5 + l_4 + \frac{c}{d} \times l_3 \tag{3}$$

Here, $\frac{a}{b}$ and $\frac{c}{d}$ are the length ratios of wing portion to the total length of the section and is taken to be our scale factor.

With the areas and beam widths known, the thickness of each of the beam section could be calculated by taking ratios with the width of the sections maintaining the assumption of wing section with a rectangular cross section. The calculated thickness data is shown in Fig. 28. We got a maximum thickness of 39.5 μm and a minimum of 3.15 μm. The mean was about 12.19 μm. Note that this thickness variation represents an equivalent mathematical model of the insect wing. The actual wing has variable thickness at different places since the veins are much thicker than the membrane. However, the overall effect of the veins is to create a wing structure which has higher flexural stiffness and thickness near the root region, just like an airplane wing.

Flexural Rigidity and Natural Frequency

The governing equation of the non-uniform cantilever wing in bending can be written as [31]

$$\frac{\partial^2}{\partial x^2}\left(EI(x)\frac{\partial^2 y(x,t)}{\partial x^2}\right) + m(x)\frac{\partial^2 y(x,t)}{\partial t^2} = f(x,t) \tag{4}$$

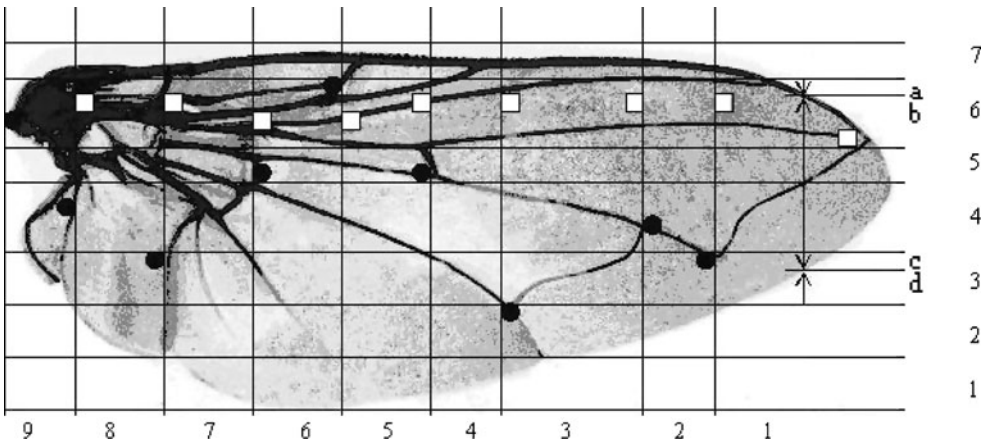

Fig. 26 Calculation of beam widths

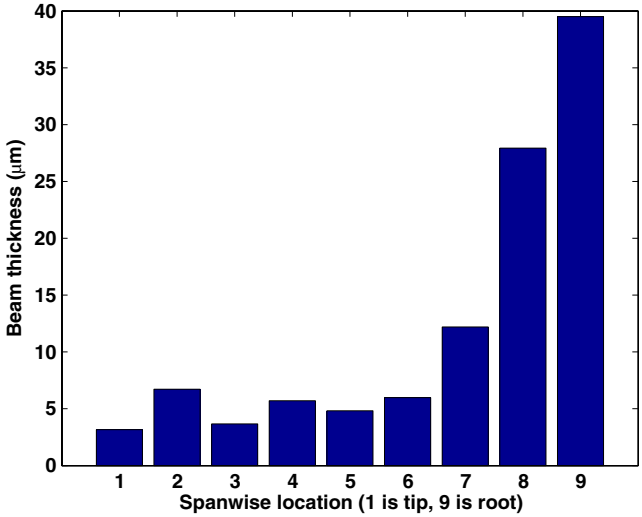

Fig. 28 Thickness variation in spanwise beam segments

where $EI(x)$ is the flexural rigidity, $m(x)$ is the mass per unit length, $y(x,t)$ is the deflection and $f(x,t)$ is the force per unit length.

The inertia at each beam segment is calculated using the formula

$$I_i = \frac{b_i h_i^3}{12} \tag{5}$$

The calculated data for inertia for the nine beam sections is shown in Fig. 29 and the mean inertia was found to be about 1.9×10^{-6} mm^4.

Inertia is taken to be constant along a beam section. We plotted a curve of inertial values against length along wingspan, assuming the inertia to be acting at the mid point of each section. The plot obtained could be approximately fit into an exponentially decreasing trend given by the equation

$$I(x) = 1.274 \times 10^{-17} e^{-1240x} \tag{6}$$

An approximation of exponential variation of flexural stiffness from wing root to tip has been observed previously [19]. Since, in our case, we assume that the Young's modulus is constant throughout the wing, inertia becomes the quantity which dominates the trend of decreasing exponentially. The plot is shown in Fig. 30.

The known values of bending stiffness at three positions of the wing are utilized in calculation of Young's Modulus (E) for the *Calliphora* wing using the integral beam equation given by

$$E = k \int_A^B \frac{x^2 dx}{I(x)}$$

$$k = \frac{F}{y_{tip}} \tag{7}$$

Here, $I(x)$ represents the second moment of inertia as a continuous function of distance and its mathematical expression is given in equation (6). The exponential fit allows us to calculate this integral analytically. This integral is evaluated thrice for three different cases for bending stiffness measurements at Basal (near Root), Medial and Distal (near Tip) locations yielding three different values of material stiffness (E). The mean of these three values is taken as the Young's Modulus for the *Calliphora* wing which comes out to be about 4.69×10^{10} Nm^{-2} which is close to the value 60 GPa used for the finite element modeling of the insect wing

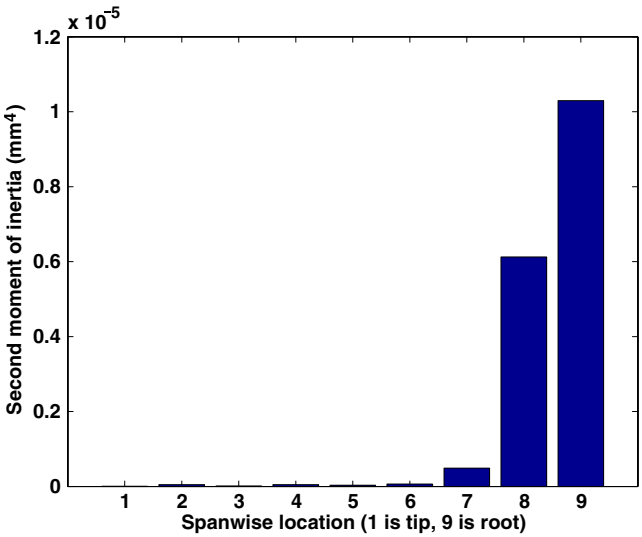

Fig. 29 Moment of inertia of spanwise beam segments

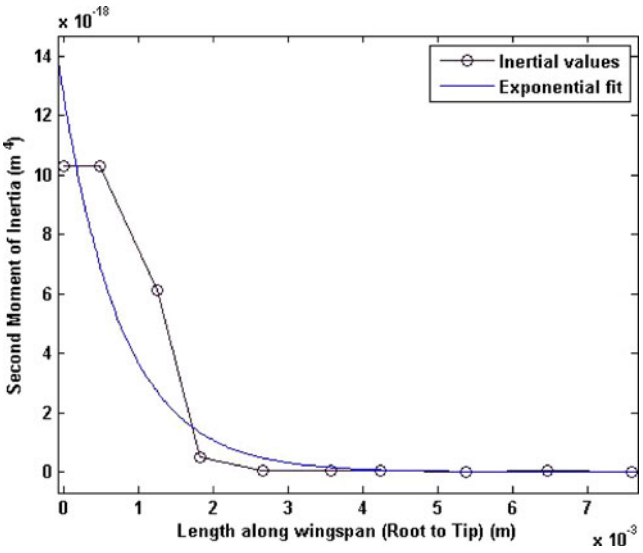

Fig. 30 Variation of inertia with length along wingspan along with the exponential trend line

[32]. Moreover, Wang et al. [14] experimentally measured the value of the Young's modulus 60–80 GPa of hindwing of the dragonfly *Pantala Flewescens*. The insect wing is a very complicated structure and the net result of the veins, membranes and corrugations on the wings is that they are quite stiff. The insect wings have thus been studied structurally by some researchers such as Wooton [17] using finite element models etc. and the fact that they have a high level of resultant stiffness has been shown. The detailed analysis of insect wings have shown the presence of chitin nanofibres the Young's modulus of which is over 150 GPa. A detailed discussion of the mechanical properties and design aspects of insect cuticles is given by Vincent and Wegst [33]. The importance of nano structures in insect wings is also mentioned by Watson and Watson [34]. While the science behind the high levels of stiffness in insect wings is not yet fully understood, our study has the limited goal of finding the resultant values for a particular insect, the *Calliphora*.

We finally calculate the flexural stiffness values for each of the beam segments of the wing by multiplying the mean material stiffness (E) obtained with calculated inertial values of each segment, i.e., $(EI)_i = EI_i$. The calculated data is shown in Fig. 31. Most of the flexural stiffness seems to be at the root of the wing. The mean of the calculated data for flexural stiffness values for all the nine beam segments gives the mean flexural stiffness as 8.92×10^{-8} Nm^{-2}. We can see that the wing is quite rigid near the root where higher structural loads are felt and are very flexible in the outbound regions. It is thus a highly flexible load carrying structure.

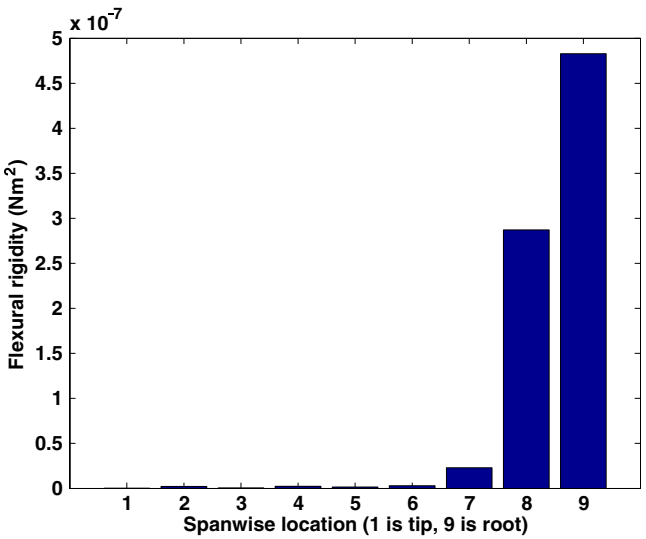

Fig. 31 Flexural rigidity variation in spanwise beam segments

Natural frequency of the cantilever wing in bending can be obtained from the homogenous part of the equation (4) which cannot be solved exactly for a non-uniform beam. Therefore, we use the finite element method to model the insect wing structure [35].

The beam is discretized into nine beam elements, with displacement and slope as nodal degrees of freedom and cubic interpolation functions. The equation of motion in discrete form for the homogeneous case is obtained after assembly of the element matrices and application of the boundary conditions, which can be written as

$$M\ddot{Q} + KQ = 0 \tag{8}$$

where M is the global mass matrix, K is the global stiffness matrix and Q is the vector of nodal degrees of freedom. For the steady state condition, starting from the equilibrium state, we seek a solution of the form

$$Q = Ue^{i\omega t} \tag{9}$$

where U is the vector of nodal amplitudes of vibrations and ω is the natural frequency. Finally, natural frequency is obtained by solving the generalized eigenvalue problem which can be expressed as

$$KU = \omega^2 MU \tag{10}$$

Flapping frequency of *Calliphora* wing is 150 Hz [27]. Natural frequency in bending is obtained 475 Hz which is 3.17 times of the flapping frequency.

Torsional Rigidity and Natural Frequency

The governing equation of the non-uniform cantilever wing in torsion can be written as

$$\frac{\partial}{\partial x}\left(GJ(x)\frac{\partial\theta(x,t)}{\partial x}\right) + f_0(x,t) = I_0(x)\frac{\partial^2\theta(x,t)}{\partial t^2} \tag{11}$$

where $GJ(x)$ is the torsional rigidity, $I_0(x)$ is mass polar moment of inertia per unit length, $f_0(x,t)$ is the applied torque per unit length and $\theta(x,t)$ is the angle of twist.

The polar moment of inertia at each beam segment was found out using the expression

$$J_i = \frac{b_i h_i}{12}\left({h_i}^2 + {b_i}^2\right) \tag{12}$$

The calculated data for polar moment of inertia for the nine beam sections is shown in Fig. 32 and it shows increasing tendency towards the root. The mean polar moment of inertia was found to be about 2.43×10^{-2} mm^4. Shear modulus (G) for the *Calliphora* wing is obtained from the following expression [36]

$$G = \frac{E}{2(1+\sigma)} \tag{13}$$

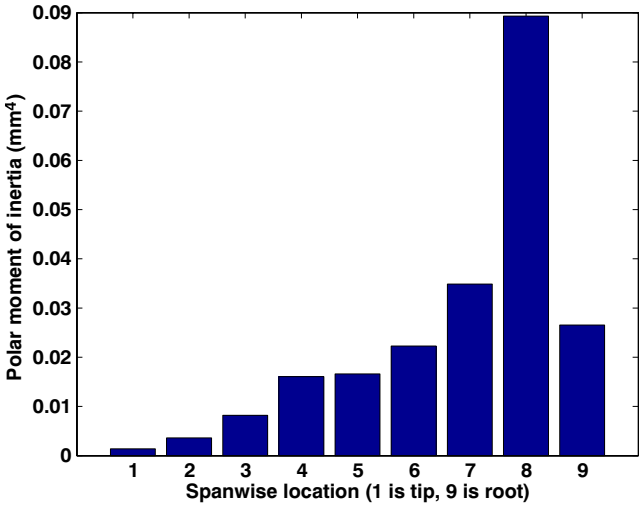

Fig. 32 Polar moment of inertia of spanwise beam segments

where, Poisson's ratio (σ) is assumed to be 0.3 [23].

Torsional rigidity values for each of the beam segments of the wing is obtained by multiplying the shear modulus (G), as obtained from equation (13), with calculated polar moment of inertia of each segment, i.e., $(GJ)_i = GJ_i$. The calculated data is shown in Fig. 33. The mean of the calculated data for torsional rigidity values for all the nine beam segments gives the mean torsional rigidity as 4.39×10^{-4} Nm^2. It can be seen from Fig. 33 that value of the torsional rigidity increases towards the root and having highest value at the location 8. This is because of maximum venation density at this location, which resists the torsional deformation.

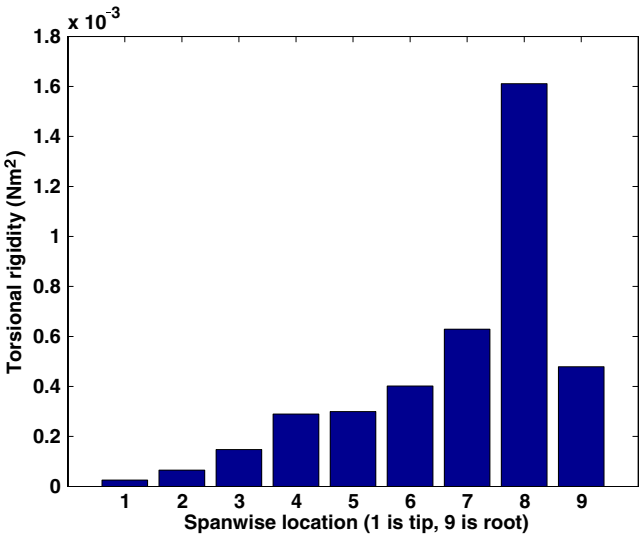

Fig. 33 Torsional rigidity variation in spanwise beam segments

Natural frequency of the cantilever wing in torsion is obtained by solving the homogenous part of the equation (11) using the finite element method. In this case, same solution procedure is followed as that of solving the governing differential equation of the non-uniform cantilever wing in bending. Natural frequency of the cantilever wing in torsion is 283 Hz which is 1.57 times of the flapping frequency of *Calliphora* wing.

The present structural modeling and analysis of the *Calliphora* wing may be useful for fundamental understanding of insect wing structure and its dynamic behavior. Moreover, the structural model may be used to study several aspects of insect wing structure such as stability [24]. In order to get a deeper understanding of the insect wing structure, the present non-uniform cantilever beam model can be revised by considering a detailed finite element model which in turn can be coupled to aerodynamic model for investigating the aeroelastic properties of the *Calliphora* wing. This we have taken up as a future work.

Some issues related to measurement uncertainty should be pointed out as they propagate into the numerical results. The Biopac load cells have a minimum 50 g full scale measurement. The accuracy of these load cells is no better than 0.1% FS, which translates to 500 μN. Given that the full range of measurements is between 2500 and 5000 μN, there is a lot of uncertainty in load measurements which are only 1% FS and will significantly effect the accuracy of the moduli measurements.

Conclusions

Experiments were performed and the mass and stiffness variation of the *Calliphora* wing was obtained. It is found that the mass per unit length is higher in the wing root and decreases towards the wing tip. The mass per unit length is highest near the leading edge of the wing and decreases towards the trailing edge. The wing shows a high level of bending stiffness near the root and there is a sharp fall in stiffness towards the tip. The wing also appears to have different bending stiffness in the upward and downward directions. The torsional stiffness is low and the elastic axis lies near the leading edge.

The wing is modeled as a cantilever beam with nine stepped segments along the wing span using experimental data. Variations of width and thickness along the cantilever wing sections are obtained for the numerical study. The inertia of the beam segments are found to decrease exponentially from root to tip and this is used to estimate the Young's modulus of the *Calliphora*

wing. Shear modulus is obtained assuming the wing is made of isotropic material and these values are in turned used for structural modeling. Flexural rigidity (EI) and torsional rigidity (GJ) are subsequently obtained and they show an increasing tendency towards the root. Natural frequencies, both in bending and torsion, are obtained by solving the homogeneous part of the respective governing differential equations using the finite element method. It is found that natural frequency in bending and torsion are 3.17 and 1.57 times higher than flapping frequency of *Calliphora* wing, respectively. The results provide a complete analysis of *Calliphora* wing structure and also provide guidelines for the biomimetic structural design of insect-scale flapping wings.

Acknowledgement The first author thanks the Alexander von Humboldt foundation for providing a fellowship for conducting part of this work.

References

1. Templin RJ (2000) The spectrum of animal flight: insects to pterosaurs. Prog Aerosp Sci 36:393–436
2. Shyy W, Berg M, Ljungqvist D (1999) Flapping and flexible wings for biological and micro air vehicles. Prog Aerosp Sci 35:455–505
3. Dickinson MH, Lehmann FO, Sane SP (1999) Wing rotation and the aerodynamic basis of insect flight. Science 284:1954–1960
4. Maybury WJ, Lehmann FO (2004) The fluid dynamics of flight control by kinematic phase lag variation between two robotic insect wings. J Exp Biol 207:4707–4726
5. Ellington CP (1999) The novel aerodynamics of insect flight: applications to micro-air vehicles. J Exp Biol 202:3439–3448
6. Ansari SA, Zbikowski R, Knowles K (2006) Aerodynamic modelling of insect-like flapping flight for micro air vehicles. Prog Aerosp Sci 42:129–172
7. Szmelter J, Zbikowski R (2002) A study of flow arising from insect wing flapping motion. Int J Numer Methods Fluids 40:497–505
8. Delauriar JD, Harris JM (1982) Experimental-study of oscillating-wing propulsion. J Aircr 19:368–373
9. Wang ZJ (2000) Vortex shedding and frequency selection in flapping wing flight. J Fluid Mech 410:323–341
10. Hall KC, Hall SR (1996) Minimum induced power requirements for flapping flight. J Fluid Mech 323:285–315
11. Okamoto M, Yasuda K, Azuma A (1996) Aerodynamics characteristics of the wings and body of a dragonfly. J Exp Biol 199:281–294
12. Wang ZJ (2005) Dissecting insect flight. Annu Rev Fluid Mech 37:183–210
13. Meyers MA, Chen PY, Lin AYM, Seki Y (2008) Biological materials: structure and mechanical properties. Prog Mater Sci 53:1–206
14. Wang XS, Li Y, Shi YF (2008) Effects of sandwich microstructures on mechanical behavior of dragonfly wing vein. Compos Sci Technol 68:186–192
15. Machida K, Oikawa T (2007) Structure analysis of the wings of anotogaster sieboldii and hybris subjacens. Key Eng Mater 345–346:1237–1240
16. Smith MJC (1996) Simulating moth wing aerodynamics: towards the development of flapping wing technology. AIAA J 34:1348–1355
17. Wootton RJ, Herbert RC, Young PG, Evans KE (2003) Approaches to the structural modelling of insect wings. Philos Trans R Soc Lond B Biol Sci 358:1577–1587
18. Combes SA, Daniel TL (2003a) Flexural stiffness in insect wings I. scaling and the influence of wing venation. J Exp Biol 206:2979–2987
19. Combes SA, Daniel TL (2003b) Flexural stiffness in insect wings II. spatial distribution and dynamic wing bending. J Exp Biol 206:2989–2997
20. Ennos AR (1988) The importance of torsion in the design of insect wings. J Exp Biol 140:137–160
21. Ennos AR (1988) The inertial cause of wing rotation in diptera. J Exp Biol 140:161–169
22. Ennos AR (1995) Mechanical behaviour in torsion of insect wings, blades of grass and other canbered structures. Proc R Soc Lond B Biol Sci 140:161–169
23. Sunada S, Zeng LJ, Kawachi K (1998) The relationship between dragonfly wing structure and torsional deformation. J Theor Biol 193:39–45
24. Rosenfeld NC, Wereley NM (2009) Time-periodic stability of a flapping insect wing structure in hover. J Aircr 46:450–464
25. Barbakadze N, Enders S, Gorb S, Arzt E (2006) Local mechanical properties of the head articulation cuticle in the beetle *Pachnoda marginata* (Coleoptera, Scarabaeidae). J Exp Biol 209:722–730
26. Langer MG, Ruppersberg JP, Gorb S (2004) Adhesion forces measured at the level of a terminal plate of the fly's seta. Proc R Soc Lond B Biol Sci 271:2209–2215
27. Deng XY, Schenato L, Wu WC, Sastry SS (2006a) Flapping flight for biomimetic robotic insects: part I—System modeling. IEEE Trans Robot 22:776–788
28. Deng XY, Schenato L, Sastry SS (2006b) Flapping flight for biomimetic robotic insects: part II—Flight control design. IEEE Trans Robot 22:789–803
29. Gorb SN, Popov VL (2002) Probabilistic fasteners with parabolic elements: biological system, artificial model and theoretical considerations. Philos Trans R Soc Lond Ser A Math Phys Eng Sci 360:211–225
30. Matushkina N, Gorb S (2007) Mechanical peoperties of the endophytic ovipositor in damselflies (Zygopetra, Odonata) and their oviposition substrates. Zoology 110:167–175
31. Rao SS (2004) Mechanical vibrations, 4th edn. Pearson Education (Singapore) Pte. Ltd., Indian Branch, Delhi
32. Bao L, Hu JS, Yu YL, Cheng P, Xu BQ, Tong BG (2006) Viscoelastic constitutive model related to deformation of insect wing under loading in flapping motion. Appl Math Mech 27:741–748
33. Vincent JFV, Wegst UGK (2004) Design and mechanical properties of insect cuticle. Arthropod Struct Develop 33:187–199
34. Watson GS, Watson JA (2004) Natural nano-structures on insects—possible functions of ordered arrays characterized by atomic force microscopy. Appl Surf Sci 235:139–144
35. Cook RD, Malkus RD, Plesha ME, Witt RJ (2005) Concepts and applications of finite element analysis. Wiley, Singapore
36. Gere JM, Timoshenko SP (1999) Mechanics of materials. Stanley Thrones, Kingston upon Thames